Rock Mech. Rock Engng. (2006) 39 (5), 395–419
DOI 10.1007/s00603-006-0083-x

Rock Mechanics and Rock Engineering
Printed in Austria

The Development of a new Numerical Modelling Approach for Naturally Fractured Rock Masses

By

R. J. Pine, J. S. Coggan, Z. N. Flynn, and **D. Elmo**

Camborne School of Mines, University of Exeter, Penryn, Cornwall, UK

Received September 12, 2005; accepted February 13, 2006
Published online March 30, 2006

Summary

An approach for modelling fractured rock masses has been developed which has two main objectives: to maximise the quality of representation of the geometry of existing rock jointing and to use this within a loading model which takes full account of this style of jointing. Initially the work has been applied to the modelling of mine pillars and data from the Middleton Mine in the UK has been used as a case example. However, the general approach is applicable to all aspects of rock mass behaviour including the stress conditions found in hangingwalls, tunnels, block caving, and slopes. The rock mass fracture representation was based on a combination of explicit mapping of rock faces and the synthesis of this data into a three-dimensional model, based on the use of the FracMan computer model suite. Two-dimensional cross sections from this model were imported into the finite element computer model, ELFEN, for loading simulation.

The ELFEN constitutive model for fracture simulation includes the Rotating Crack, and Rankine material models, in which fracturing is controlled by tensile strength and fracture energy parameters. For tension/compression stress states, the model is complemented with a capped Mohr-Coulomb criterion in which the softening response is coupled to the tensile model. Fracturing due to dilation is accommodated by introducing an explicit coupling between the inelastic strain accrued by the Mohr-Coulomb yield surface and the anisotropic degradation of the mutually orthogonal tensile yield surfaces of the rotating crack model. Pillars have been simulated with widths of 2.8, 7 and 14 m and a height of 7 m (the Middleton Mine pillars are typically 14 m wide and 7 m high). The evolution of the pillar failure under progressive loading through fracture extension and creation of new fractures is presented, and pillar capacities and stiffnesses are compared with empirical models. The agreement between the models is promising and the new model provides useful insights into the influence of pre-existing fractures. Further work is needed to consider the effects of three-dimensional loading and other boundary condition problems.

Keywords: Rock mass strength, numerical modelling, 3D fracture model, mine pillars.

1. Introduction

The determination of rock mass strengths for design of underground excavations is a seemingly straightforward task but involves many complexities and compromises.

In essence, as explained by Starfield and Cundall (1998), the key components of any satisfactory modelling approach are data and understanding. In a joint venture between the Camborne School of Mines, the University of Wales, Swansea and other collaborators, we are creating a new numerical modelling approach that maximises the use of feasibly available data and the understanding of the failure process of a naturally fractured rock mass as induced stresses arise through excavation.

This paper provides details of the concepts involved and progress to date with the data capture and synthesis (for one mine site in particular) and with initial geomechanical model development and trial runs. Whilst the scope of the model extends to all elements of underground excavations in rock (e.g., pillars, hangingwalls, tunnels, and block cave zones), the initial work has been concentrated on pillars. Some initial geomechanical modelling has also been undertaken to simulate block caving, with a simplified approach to fracture representation, and the approach is also applicable to rock slopes, where some initial geomechanical modelling results have already been published (Eberhardt et al., 2004; Stead et al., 2004).

The proposed model seeks to maximise the use of accessible data, notably the intact rock properties and the orientation, persistence and intensity of fracturing for direct use in the geomechanical model, whilst explicitly accounting for size and shape (scale) effects. The platform for data capture and synthesis is the program FracMan (Dershowitz et al., 1998; www.fracman.golder.com), which has been used on numerous projects in civil, mining, and oil and gas projects where a good understanding of the effects of fracture networks is required. The geomechanical model is produced using the program ELFEN (Klerck et al., 2004; Owen et al., 2004; www.rockfield.co.uk), which was originally used for the dynamic modelling of brittle solids (e.g., ceramics) but has found increasing use in rock mechanics (Coggan et al., 2003; Cai and Kaiser, 2004).

2. Development of the Rock Mass Fracture Network Model

2.1 Data Capture and Synthesis

FracMan characterises each fracture set within a single structural domain using statistical distributions to describe variables such as the orientation, persistence and spatial location of the fractures. The approach taken in FracMan is to maximise the utility of fracture data from mapping of exposed surfaces and boreholes. The complete range of options in FracMan far exceeds the scope of this paper. However the key components and capabilities used in the current project are as follows:

(i) From mapping of windows (2D surfaces), scanlines and boreholes (1D line data), statistical data are obtained for the orientations, persistence, intensity (spacing), and other relevant properties of fractures on a set by set basis.

(ii) Orientations are defined typically by Fisher distributions with mean and standard deviation values for dip and dip direction, by analysis of the data for specific sets.

(iii) Persistences are defined typically by log normal or negative exponential distributions and the best distribution can be determined by statistical test (chi-squared).

(iv) Intensity of a fracture set is described by two main measures: P_{21} is defined as the mean total length (m) of fracture within a given area (m^2). This can be determined directly from mapped windows by simply summing the lengths of the fractures and dividing by the area of the window. P_{32} is defined as the total surface area of fractures per unit volume. It cannot be measured directly but can be determined by the synthesis of the fracture data in FracMan. The subscript notation first gives the sample dimension in which fractures are measured or simulated, i.e., 1 represents a line, 2 an area and 3 a volume; and second the measured or simulated parameter for a group or set of fractures, i.e., 0 represents spacing, 1 represents length and 2 area. As seen in Figs. 1 and 2, P_{21} is direction dependent, but P_{32} is direction independent. Both P_{21} and the P_{32} are scale independent. For each orientation, there is a direct relationship between P_{32} and P_{21} i.e., $P_{32} = C_{32}\, P_{21}$. The constant C_{32} is obtained from modelling with different numbers

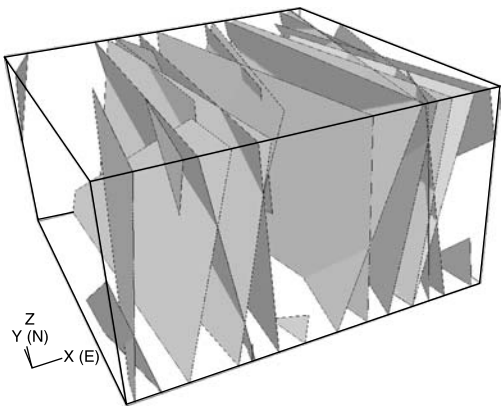

Fig. 1. Synthetic realisation of fracture set 1a generated within a region equivalent to a Middleton pillar. $P_{32} = 0.79\,m^2/m^3$ for this rock volume

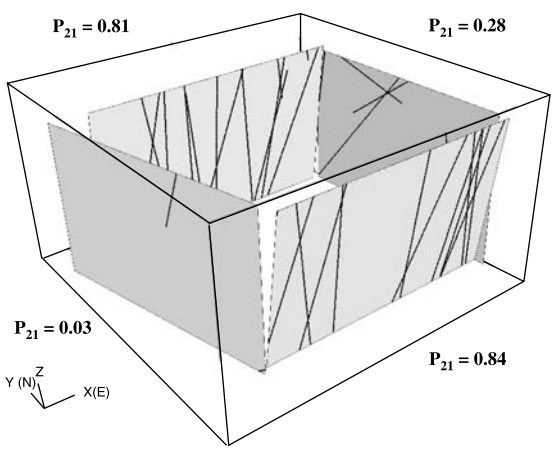

Fig. 2. Traces of the fractures from Fig. 1 on planes corresponding to those mapped at Middleton showing the clear anisotropy of the P_{21} (m/m^2) values

of fractures that give a linear relationship between simulated values P_{32} and P_{21}. The best estimate of actual P_{32} is then given by C_{32} multiplied by the mapped P_{21}.

(v) Fractures are polygons of zero thickness with multiple sides but typically 4 or 6 sides are selected. Whilst a good default is that the polygons are equi-dimensional and planar, they can be elliptical with a defined orientation for the major axes. Zhang et al. (2002) described analytical methods for determining fracture shapes and dimensions from mapping windows and used FracMan to simulate and validate their approach.

(vi) There are several options for locating fractures in the 3D fracturing model. The default option is the Baecher model and this is based on a random Poissonian distribution of fracture centres in 3D space. Other models allow for clusters, fractal distributions etc. For the current project for the locations mapped to date, the Baecher model appears satisfactory.

(vii) Model building proceeds on a set-by-set basis. Fractures are generated using a stochastic selection of the orientation, diameter, and spatial location of the fracture such that the prescribed statistical distributions of the fracture sets are adhered to. Generation continues until a pre-defined value of P_{32} has been achieved. Fracture intersections or truncations can be controlled on a set-by-set basis with dominant and subordinate sets (e.g., bedding planes may predominate over cross fractures which are truncated by the bedding planes).

(viii) Model validation is achieved by taking 2D slices through the model along planes corresponding to the mapped windows and comparing the pattern and intensity (P_{21} and the number of fractures per unit area) of the fracture traces (from all sets) with those measured in the equivalent mapping window. Again, statistical tests are available to determine which pattern of fractures (e.g., Baecher or otherwise) gives the best fit.

Since the above process is stochastic, there are infinitely many possible realisations of the 3D fracture system based on the mapped data. Indeed the mapping process is itself random by the nature of how fractures are presented in available windows. However, except for very explicit modelling of an individual fracture or simplified sets of fractures, which cannot be wholly representative, the stochastic approach provides the best option for creating realistic geometric models of fracturing.

While it is relatively easy to create many realisations from FracMan, under current limitations of computing capacity, only a limited number can be subsequently used for geomechanical modelling. However, we consider that for many practical cases, such as the pillars we have described, there is sufficient fracture intensity that the variability in mass strength/pillar load capacity, particularly in 3D, can be captured with a limited number of geomechanical models. An objective of this project is to examine the variability of pillar capacity in relation to empirical experience in choosing factors of safety. Experience with modelling fluid flow in fracture networks created by using the FracMan approach described above, again demonstrates that the variability for well-connected networks is within practically usable ranges (Dershowitz, 1992; Dershowitz et al., 2001).

A notable result of the synthesis, which is undoubtedly true in real rock masses, is that few complete blocks are formed. A module, FracBlock, is available within

FracMan to determine the formation of such complete blocks. This is not particularly important for hydraulic considerations (fracture network connectivity), but has obvious implications for geomechanical modelling. For such a rock mass to fail under induced stresses, the processes involved are likely to involve extension of existing fractures or growth of fractures in the adjacent intact rock, or both. The failure process would not initially involve the high magnitude of immediate displacement made possible by the presence of complete blocks.

2.2 Mapping Considerations

In a research project considerable effort can be devoted to obtaining the best possible data sets from field mapping and borehole logging, in excess of what would be practical in many other projects. Whether a project is research-based or otherwise, it is important to be efficient in capturing sufficient data for a meaningful model. In an operating mine there are several practical considerations that affect data capture, including phasing of mining operations, lighting, ventilation, access to mappable surfaces and supervision aspects of health and safety. The data has to be obtained within these constraints and is therefore imperfect. For the current project the following approach has evolved:

(i) Locations are selected for mapping which are representative of the rock mass element to be modelled (i.e., within the same geological/geomechanical domain).

(ii) Fracture orientations are measured directly with a suitable compass-clino over a wide area of the domain to determine if there are any systematic or sudden (fault-induced) trends.

(iii) Window mapping is undertaken within at least two windows with orientations approximately at right angles (to ensure all fracture sets are adequately represented).

(iv) Mapping locations are selected preferably where air quality is good enough to permit flash photography.

(v) For determination of fracture persistence, mapping is undertaken at two scales. For detailed data, windows are typically 2 m high (within direct physical reach) and several metres wide. Beyond the window, within range of flash photography the longer fractures are recorded, including those that extend beyond the initial 2 m high window. Types of fracture termination are recorded with one end, both ends or neither end terminating within the window or truncated against other fractures. These data are used to determine the persistence trends and possible distributions (Zhang and Einstein, 2000), and to incorporate truncation percentages within the synthesised model.

(vi) A minimum cut-off for fracture length during mapping is a practical constraint for both the mapping effort and the subsequent geomechanical model run times. A value of 0.5 m has been used initially for pillars with dimensions of typically 10 times this size.

(vii) Checks are made on fracture spacing using scanlines, which are orientated approximately normal to obvious fracture sets. The spacings of the longer fractures are determined from scaling the photographic data. In the data captured so far the mapped spacing distribution is quite close to negative exponential, consistent with a model assumption of Poissonian distribution in 3D space.

Fig. 3. Typical view of Middleton Mine

2.3 Results of Rock Mass Mapping and Classification at Middleton Mine

Through our collaboration with the industrial minerals company, OMYA, we have had access on several occasions to their limestone mine at Middleton in Derbyshire, UK, and also to their marble mine at Vipiteno, Italy, near the Brenner Pass border with Austria (Pine et al., 2004). In this paper we concentrate on the mapping and modelling of the Middleton Mine pillars.

Middleton Mine is a classic square room and pillar mining operation with drift access working mostly under a cover of about 100 m. Pillars are planned for nominal 16 m × 16 m dimensions in plan with rooms 14 m wide. Actual pillars are usually

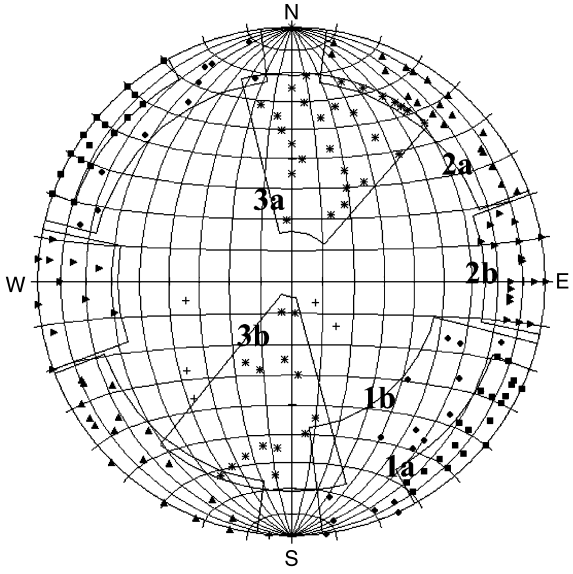

Fig. 4. Lower hemispherical stereoplot of the sets of poles to the fractures mapped at Middleton Mine

smaller, due to overbreak. In single pass operations, rooms are created up to 8 m high, but double height rooms are created in suitable ground. Figure 3 shows a typical view in the mine. The mine area is divided by several normal faults across which there can be significant vertical displacement. The orientations of the major faults determine the layout of the rooms.

The excavation is within the payable Hoptonwood limestone. This is a massive cream-grey, coarse-medium grained carboniferous limestone, approximately 80 m thick. It is interspersed with clay wayboards (seams) of volcanic origin up to 0.5 m thick. All strata are very continuous with remarkably consistent thickness and low dip

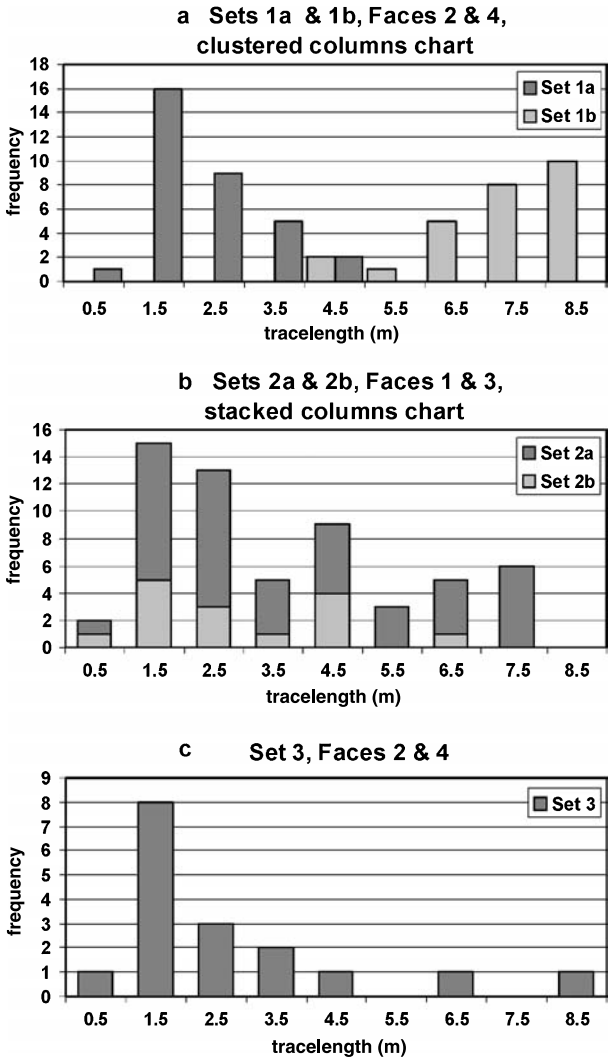

Fig. 5. Histograms of trace lengths measured for each fracture set in two parallel windows that give the maximum number of data points

(less than 5°). The unconfined compressive strength ranges from 40 to 65 MPa (Bearman, 1991) and the Young's modulus is about 20 GPa. Rock mass classification results in RMR values of about 60 to 70 and Q values of 6 to 17. The main spatial difference in rock mass quality from location to location is due to the intensity (spacing) of fractures.

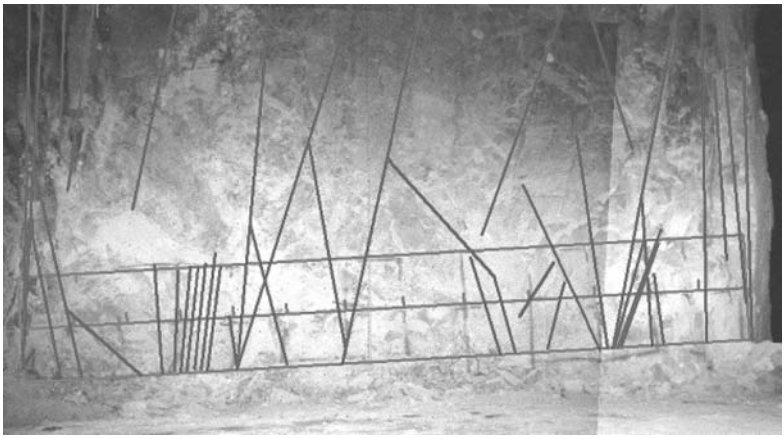

Fig. 6. Interpreted fractures on a mapped pillar face at Middleton Mine, facing NW. The pillar face (Face 1) is 13×7 m. The 2 m high panel at the base of the pillar, where detailed mapping was undertaken, is also shown

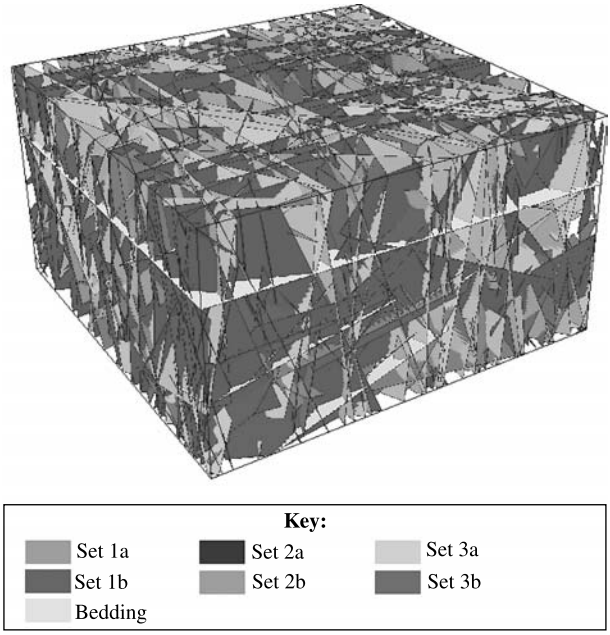

Fig. 7. FracMan 3D model of a Middleton pillar. The dimensions are approximately $14 \times 14 \times 7$ m high

Figure 4 shows a stereoplot of the fractures mapped at Middleton. There are two major sub-vertical, medium spaced (0.5 to 1.0 m) fracture sets: set 1 strikes roughly NE–SW and set 2 N–S to NW–SE. Set 3 is a more widely spaced (2 to 4 m) set striking W–E and dipping at about 45° to both North and South (bivariate distribution). The near horizontal bedding planes are widely spaced (2 to 4 m). From mine wide surveys, the orientations of fractures appear consistent with only localised effects at faults.

Based on mapped tracelengths, as shown in Fig. 5, set 1 is divided into two sub-sets. Set 1a comprises long fractures that extend over the full height of the face with a mean dip of 87° towards 308°. Set 1b comprises shorter fractures (maximum mapped tracelength 4.7 m) of a similar, but more dispersed, orientation, as shown in Fig. 4. Set 2 is also divided into two sub-sets, based solely on orientation, again as shown in Fig. 4. Set 2a has a mean dip of 88° towards 038°; set 2b has a mean dip of 89° towards 270°. While sets 2 and 3 have essentially log-normal length distributions, as often encountered in the field, clearly set 1a/1b shows a bimodal distribution due to the relatively high number of long traces (or low number of short traces) in set 1a. The geological reason is not known but this is a true reflection of the field observations.

The mapping was concentrated on two adjacent pillars, providing two windows in each of two near perpendicular orientations. A total of 226 fractures was mapped. The results of the mapping in one of the windows and the photography outside the window are shown in Fig. 6. Using FracMan to analyse and synthesise the data from all four windows, the 3D simulation of a mass representing one of the pillars is shown in Fig. 7. A comparison between a mapped window and synthesised panel of the same orientation is shown in Figs. 8 and 9. Using the approach described above the P_{32} values for the two main sub-vertical fracture sets were 1.67 and 1.80 m^2/m^3 contributing to a total of 3.86 m^2/m^3, including bedding planes. These values represent a best estimate, which in this case is quite dependent on the sparsity and variability of the mapped fractures in the four windows. For a more intensely fractured rock mass mapped within the same window, or alternately for a larger window size, the model and total P_{32} will be increasingly robust.

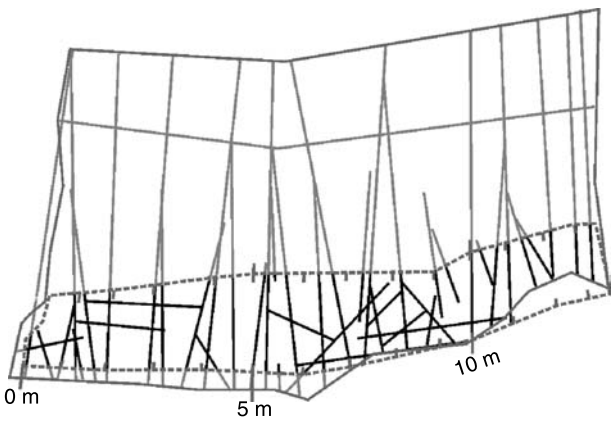

Fig. 8. Mapped Pillar Face 2, facing SW. The 2 m high panel mapped in detail is highlighted

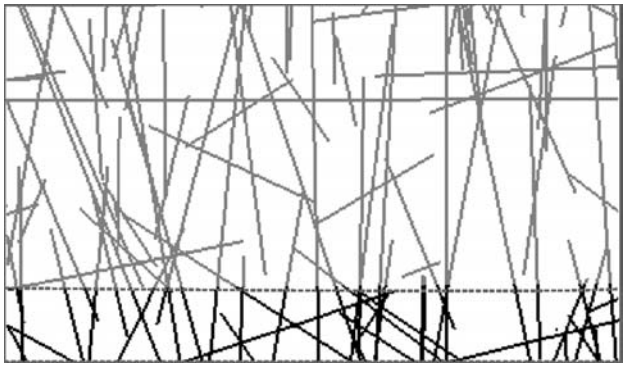

Fig. 9. FracMan simulated fractures on a Pillar Face 2 for one realisation of fracturing at Middleton. The face is 14 m wide × 7 m high

In addition to the mapping at Middleton Mine, in collaboration with 3dT, Skanska UK and OMYA, we plan to undertake tomographic mapping of a pillar as it is created and loaded. From work undertaken by 3dT Skanska at Silbury Hill (a conical shaped iron age burial mound), it was observed that higher P-wave values associated with more confined strata gave clear expression in the tomographic images. The results of an initial survey on one of the mapped pillars are shown in Fig. 10. This shows an outer ''ring'' with a P-wave velocity of less than 1000 m/sec, about 1 m thick, a somewhat thicker and uneven intermediate ring between 1000 and 2000 m/sec and an inner core with a range of 2000 to 2500 m/sec. These results are consistent with the loading profiles seen in the pillar models presented later.

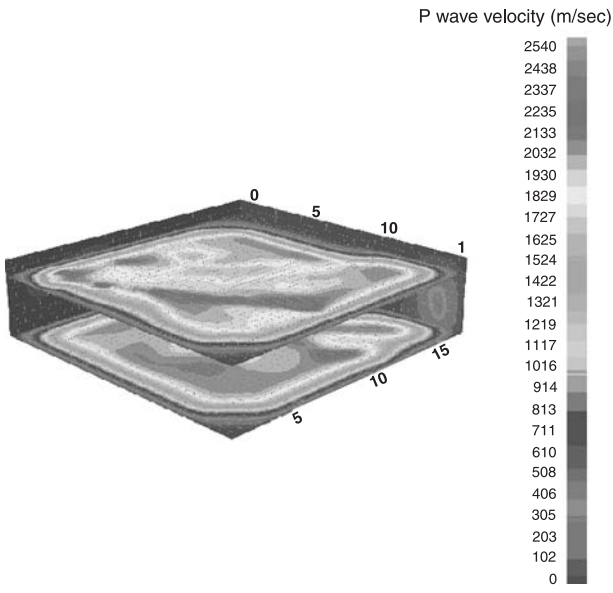

Fig. 10. Results of an initial seismic tomographic survey on one of the mapped pillars at Middleton Mine

3. Development and Implementation of the Geomechanical Modelling Approach

3.1 Basis of Geomechanical Modelling

The geomechanical modelling is undertaken using the program suite ELFEN, which employs a combination of finite and discrete element approaches. While it can be run for three-dimensional initial continuum models, work to date in pre-fractured rock has been in two-dimensions. It is intended that some three-dimensional modelling will be completed in the current phase, but the extent will depend on the resolution of some programming issues, the extent of capturing the mapped complexities of the three dimensional pre-fracture geometries, and progress towards development of parallel coding.

The quasi-brittle fracture capability of ELFEN has been developed through application to a large number of materials including metals, ceramics, and numerous other geomaterials including concrete and rock (Owen et al., 2000 and 2001). In modelling quasi-brittle materials, ELFEN provides a variety of constitutive models including the Rotating Crack, and Rankine tensile smeared crack descriptions, in which material strain softening is fully governed by the tensile strength and specific fracture energy parameters. Both of these models have the advantage of being based on parameters that can be determined experimentally under laboratory conditions. All fracture extensions and new fractures develop in Mode I, i.e., tension only. All existing fractures and new fracture surfaces, once created, are given the same Mohr-Coulomb shear strength parameters c_f and ϕ_f. Particular fracture sets may, in principle, have clearly different surface morphologies, hence different shear strengths. This has not been included in the current model.

In both the Rotating Crack and Rankine models, plasticity evolves through degradation of the elastic modulus in the directions of the principal strains. For the Rotating Crack approach the degradation of the elastic modulus in each principal direction is totally independent of the other principal components, therefore providing a completely anisotropic material description. For the Rankine model, initiation of material strain softening in all three of the principal directions is controlled solely by the major principal stress term. Both of these models can be applied within a standard continuum finite element framework whereby material failure is confined to the concept of material strain softening, or they can be explicitly coupled to the fracture insertion algorithm within ELFEN to introduce physical cracking of material.

For tension/compression stress states, the widely used Mohr-Coulomb failure criterion has been adapted and coupled with a fully anisotropic tensile smeared crack model, known as the compressive fracture model (Klerck, 2000; Klerck et al., 2004). The Mohr-Coulomb criterion is able to recover the salient features of the quasi-brittle response, including dilation. In addition, material softening due to dilation is accommodated by introducing an explicit coupling between the inelastic strain accrued by the Mohr-Coulomb yield surface and the anisotropic degradation of the mutually orthogonal tensile yield surfaces of the tensile smeared crack approach. The developed compressive fracture model represents a phenomenological approach in which micro mechanical processes are only considered in terms of the average global response. Local isotropy of strength in compression is justified by assuming uniform material

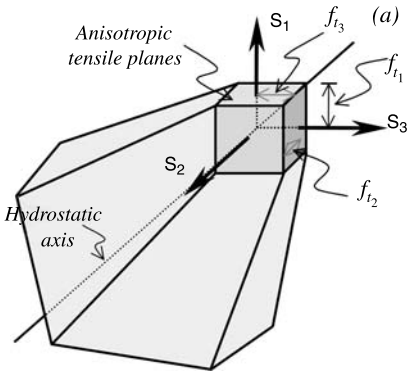

Fig. 11. The compressive fracture model, the isotropic Mohr-Coulomb yield surface with softening anisotropic tensile planes (after Klerck, 2000)

heterogeneity, while accumulation of inelastic strain and associated degradation of the tensile strength is necessarily anisotropic and dependent on the loading direction. The yielding surfaces defining the compressive fracture model are presented in Fig. 11.

The basic Rotating Crack and Rankine model formulations, together with the more advanced compressive fracture model have been rigorously applied and validated for both 2D and 3D configurations, including punch tests and borehole breakouts. These demonstrate that the model is able to quantitatively predict the appropriate load-displacement response in both weak (limestone) and strong (granite) rocks, where the failure mechanisms are distinctly different (Klerck, 2000). In addition, the accurate evolution of the discrete fracturing profile in situations comprising of a variety of compressive and tensile stress states has also been considered.

The propagation of fractures, hence a major part of rock mass behaviour in 2D and 3D, is controlled by stress intensity factors related to the scale of the existing fractures (extension of existing) or flaws in intact rock (creation of new fractures). In weaker rocks, the influence of fractures is less important, and this can be accommodated by lower values of fracture toughness and tensile strength with greater importance of Mohr-Coulomb or Hoek-Brown behaviour of the intact rock.

3.2 Transfer of Fracture Geometry Data from FracMan to ELFEN

The methodology for transfer of the fracture geometry data from FracMan to the finite/discrete element ELFEN model includes the following essential steps:

- The fracture geometry data are exported from the Fracman system in files defining fracture planes within a rock mass on a full three dimensional basis. These planes may intersect at arbitrary angles and do not normally traverse the entire region. This information is imported to a specific solid modelling interface module in ELFEN in which the joints are represented as lines for 2D and planar surfaces for 3D situations.
- Each fracture surface is then assigned interface properties. Normally this would be on the basis of geologically defined sets identified in FracMan.

- Fracture entities are first constructed independently as a network, accounting for intersections of lines or surfaces, including part intersection of surfaces in 3D and the intersection with material region boundaries.
- Once the network has been constructed these are embedded within the solid model of the rock mass by inserting fractures with both sides of the fracture represented as free surfaces. Special cases need to be considered when fractures or faults run along material interfaces or through rock strata with discontinuous properties, etc., to ensure correct insertion of properties and assignment of operations. This solid model is then discretised to provide a finite element mesh using automatic mesh generation techniques employing triangular elements in 2D and tetrahedra for 3D problems. During this meshing procedure, algorithms are employed to ensure that either excessively small or "sliver" elements are not formed, due to either (a) very closely spaced joints – in which case the two joints are merged or (b) termination of a joint in close proximity to another joint – in which case the nodes defining this near interception are "snapped" together. In such cases one of the fractures is displaced, preserving the overall intensity of fractures (P_{21} or P_{32}) and maintaining the orientation of the displaced fracture. These adjustments are considered to have negligible impact on the overall geomechanical behaviour of a system of multiple fractures.
- A final important requirement is to ensure that equilibrium conditions are satisfied when initial geostatic loading conditions are applied. The algorithms developed allow the contact conditions between the two surfaces of any joint to build up in a controlled manner avoiding excessive force imbalance at any stage before the full contact forces have developed.

3.3 Rock Mass Properties and Initial Geomechanical Modelling

The Middleton Mine fracture distribution model has been incorporated in a 2D ELFEN pillar model, as described above, to examine a number of issues related to loading and failure. A number of different cross sections in the same orientation were taken from the FracMan model and used to examine pillars of 2.8, 7 and 14 m wide $\times$ 7 m high. The pillars were simulated as if subject to uniaxial laboratory loading. Later in the project it is intended to create pillars by staged excavation within pre-stressed 2D and 3D solids containing the same fracture systems.

In the basic models, the properties of the intact rock and rock fractures were as shown in Table 1. These values were derived from a combination of laboratory measurements on the Hoptonwood limestone and typical values for similar limestones from the literature. In these models the smallest element size was 0.2 m. The properties of the platens and the rock/platen contact were as shown in Table 2.

For the Mohr-Coulomb model of the intact rock, internal values of cohesion, c_i, and friction, ϕ_i, are also required. These were determined from the value for σ_{ci} of 48 MPa and Hoek-Brown parameters of $s = 1$ and $m_i = 10$ (typical for this limestone), over a limited range of confining stress, using the program RocLab with RMR set to 100 (Hoek et al., 2002). The resulting values were $c_i = 9.2$ MPa and $\phi_i = 45^\circ$, although slightly different values might be appropriate depending on the actual confining stress profile in the pillar. This could be examined by iteration within the pillar modelling but is considered to be of secondary importance at this stage.

Table 1. Intact rock material and fracture values for pillar modelling

Property	Unit	Value
Intact rock material		
Unconfined compressive strength, σ_{ci}	MPa	48
Fracture energy, G_f	Jm^{-2}	19.5
Tensile strength, σ_t	MPa	3.8
Young's Modulus, E	GPa	27.5
Poisson's ratio, ν		0.23
Density, ρ	kgm^{-3}	2600
Internal cohesion, c_i	MPa	9.2
Internal friction, ϕ_i	degrees	45
Rock fracture		
Surface cohesion, c_f	MPa	0.1
Surface friction, ϕ_f	degrees	30
Normal stiffness	GPa/m	1.0
Shear stiffness	GPa/m	0.2

Table 2. Parameter values for pillar loading platens

Property	Unit	Value
Young's Modulus of platen	GPa	200
Poisson's ratio of platen		0.3
Density of platen	kgm^{-3}	7860
Rock/platen cohesion	MPa	0.1
Rock/platen friction	degrees	30
Rock/platen normal stiffness	GPa/m	1.0
Rock/platen shear stiffness	GPa/m	0.2

Table 3. Rock mass rating (RMR/GSI) values for pillar modelling

Property	Value	RMR rating
UCS of intact rock material	50–100 MPa	7
RQD	50–75%	13
Spacing of discontinuities	0.3 to 1 m	20
Condition of discontinuities	smooth, unfilled	20
Groundwater	none	10
Adjustment for orientation	none	0
Total		70

Based on the mapped rock fracture patterns and the above properties, an RMR value was determined as shown in Table 3. This is based on the 1976 RMR classification, which is equivalent to GSI for this type of rock mass (Hoek et al., 1995). The range in possible GSI values for the pillar based on the qualitative/descriptive approach is about 60 to 70 (blocky to massive rock with fair good surface conditions).

3.4 Modelling Results

Many simulations were undertaken with slender 2.8 m wide $\times$ 7 m high pillars, as these demonstrated critical aspects of the failure process at earlier stages than for

wider pillars and computer run times were significantly less. A limited number of simulations was also completed for the 7 m wide pillars and two simulations were completed for the 14 m wide pillars. All simulations were conducted in plane strain. The loadings were in two stages, with an initial stage of gravity loading followed by a constant strain rate control on platen closure. In all cases the pre-fractured rock was extended throughout the full external height of the rock pillar. A thin layer of intact rock was included between the fractured rock and the platen to limit observed numerical instability. This is considered to have had negligible effect of overall pillar behaviour.

Figure 12 shows the fracture evolution in several stages of loading (P1 to P5) for a 2.8 m wide pillar (model A) with the properties given in Table 1. The stages are shown in the stress-strain relation of Model A in Fig. 13.

The initial fractures (from the FracMan model) extend very little until stage P1, when the average axial stress is about 1.2 MPa. Note that for this and following values the average axial stress is determined from the total load divided by the initial pillar width. In addition to fracture extension there are a few new fractures created and the beginning of block ejection from the pillar surface. By stage P2 (about 2 MPa) a clear load-bearing core is established with the outer layers of rock becoming detached.

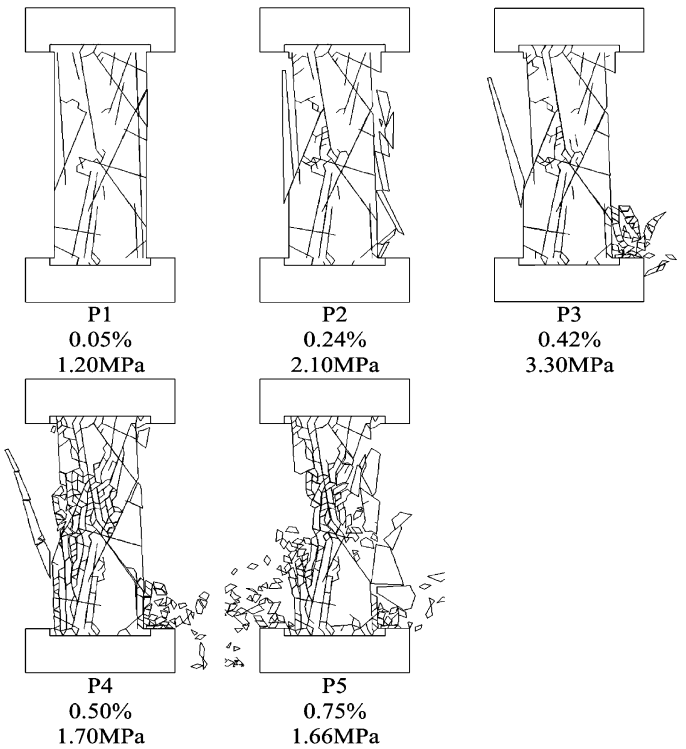

Fig. 12. Fracture evolution in several stages of loading (P1 to P5) for a 2.8 m wide pillar (model A) with the properties given in Table 1. The average axial strain and stress values are shown in Fig. 13

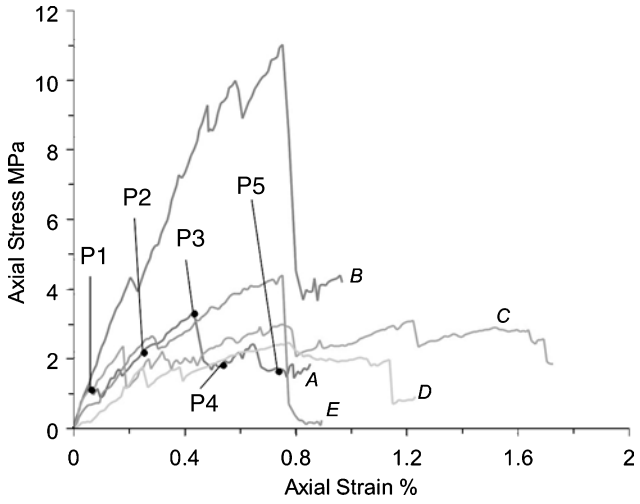

Fig. 13. Average stress/strain plots for 5 individual pillar models each 2.8 m wide. All models have fracture intensity (P_{21}) in the range 2.4 to 2.6 m/m^2 except for model B, which has a reduced value of 1.8 m/m^2. P1 to P5 refer to the sequence of loading stages illustrated in Fig. 12

Within the core new fracturing occurs in local positions where the longer pre-fractures appear to channel stress concentrations. By stage P3 (peak) at nearly 3.3 MPa there is further ejection and a limited increase in local fracturing. After the peak, in stages P4 and P5, the remaining core is almost wholly consumed by local fracturing. It is evident that, partly due to the initial pre-fracture pattern, the overall failure behaviour is asymmetric.

Other simulations were undertaken with similar models but varying some of the key properties. While all variations had some effect, the key sensitivities were due to the actual fracture pattern (and degree of asymmetry) and the values of the fracture normal and shear stiffnesses. In general the higher stiffnesses led to higher overall pillar stiffnesses but lower average peak stresses. The higher stiffnesses, which caused more ''locking-up'', tended to limit the generation and release of the larger blocks and increase the amount of local fracturing.

Figure 13 shows the average stress-strain plots for 5 individual pillar models each 2.8 m wide. All the models had a fracture intensity (P_{21}) in the range 2.4 to 2.6 m/m^2 except for model B which had a reduced value of 1.8 m/m^2. The models were taken from different sections of a synthesised 14 m wide pillar model based on the original fracture statistics for the Middleton model. The initial fracture patterns are show in Fig. 14. The range in peak strengths is from about 3 to 4 MPa, except for model B, which has a peak of about 11 MPa. The overall stiffnesses of the pillars are also quite variable, typically in the range 0.4 to 1 GPa with model B at about 2 GPa. Figure 15 shows the axial stress profile for model A through the sequence of loading stages, P1 to P5. The asymmetric nature of the load development is evident.

Figure 16 shows the initial fracture pattern in one of the 7×7 m model pillars, Fig. 17 shows the overall stress-strain behaviour and fracture evolution and Fig. 18 shows the fracturing near peak stress. Also included in Fig. 18 are the contours of

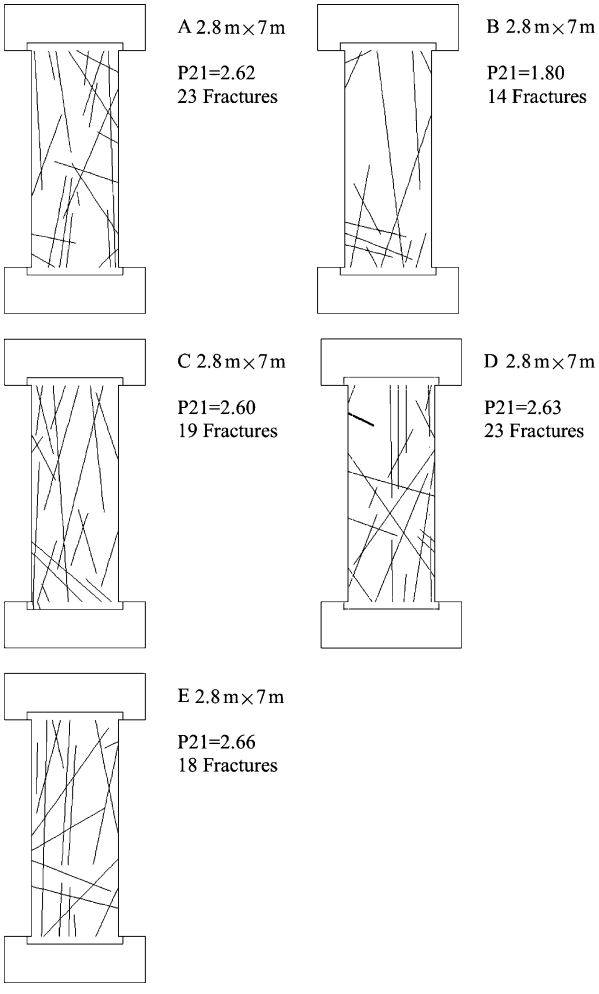

Fig. 14. Initial fracture patterns for the 5 individual pillar models, each 2.8 m wide and 7 m high. Also indicated are the associated P_{21} value (m/m^2) and the number of fractures

induced yy (axial direction) stress (Pa) showing the concentration of loading in the core of the pillar. Similar results are shown in Figs. 19 and 20 for a 14×7 m pillar. For the 7×7 m and 14×7 m pillar the peak strengths and deformation modulus values were 15 and 22 MPa and 2 and 2.5 GPa, respectively.

Using the GSI/RMR value of 70, from Table 3, a σ_{ci} value of 48 MPa from Table 1 and an m_i of 10, the RocLab approach to the determination of mass strength (Hoek et al., 2002) gave a rock mass uniaxial compressive strength σ_c of 9.0 MPa, and a partially confined rock mass compressive strength, σ_{cm} of 13.5 MPa. The former is insensitive to the value of m_i, and the latter varies between 12.4 and 15.8 MPa for a range of m_i of between 8 and 15. The confining stress range for the latter is between the tensile strength and 1/4 of the compressive strength of the intact material (see Hoek et al., 2002 for

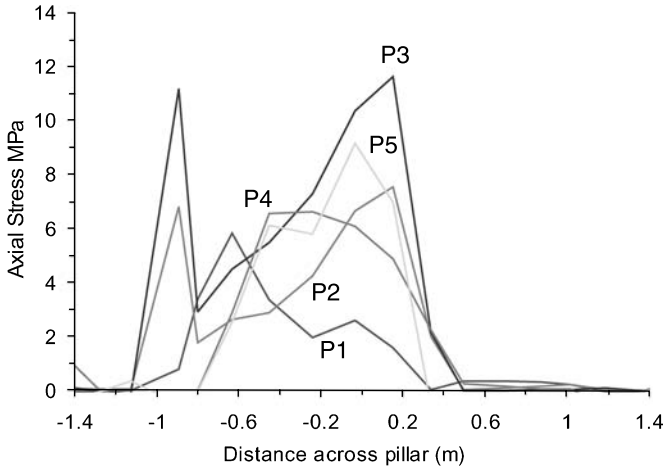

Fig. 15. Axial stress profile for model A through the sequence of loading stages, P1 to P5, illustrated in Fig. 12. The asymmetric nature of the load development is evident

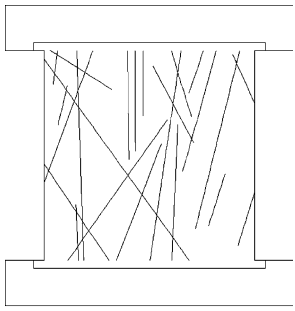

Fig. 16. Initial fracture patterns for one of the 7 m × 7 m model pillars, with a P_{21} value of 1.8 m/m^2 and 24 fractures

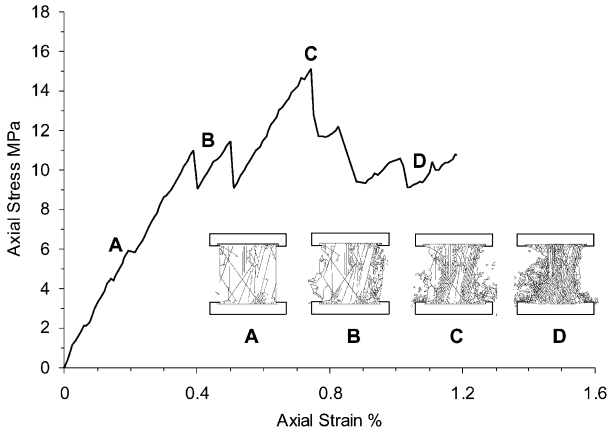

Fig. 17. Stress-strain behaviour for 7 m × 7 m pillar in Fig. 16 showing fracture states at different stages of loading

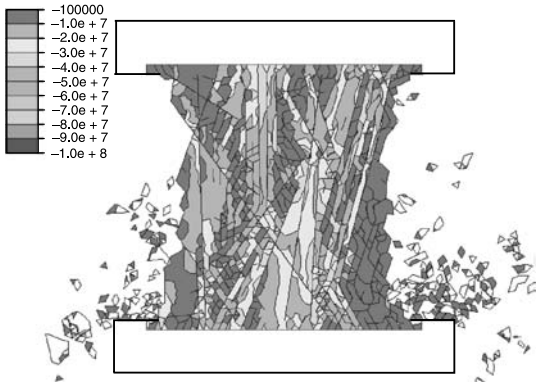

Fig. 18. Fracturing near peak stress, at an average axial stress of 15.15 MPa and 0.74% average axial strain for the 7 m × 7 m pillar model illustrated in Figs. 16 and 17. Also included are the contours of induced yy stress (Pa), in the axial direction (compression negative), showing the concentration of loading in the core of the pillar

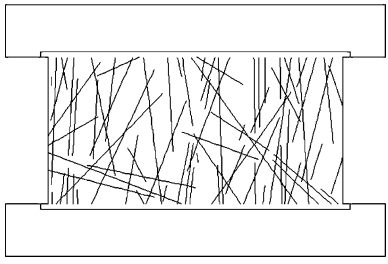

A 14 m × 7 m
P_{21} = 2.60
77 Fractures

Fig. 19. Initial fracture patterns for one of the 14 m × 7 m model pillars. Also indicated are the associated P_{21} value (m/m^2) and the number of fractures

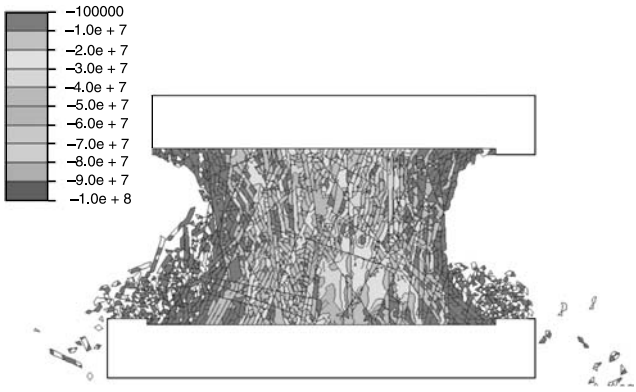

Model A 14 m × 7 m
Strain % 1.19
Stress MPa 22.42 (Peak)

Fig. 20. Fracturing near peak stress for the 14 m × 7 m pillar model illustrated in Fig. 19. Also included are the contours of induced yy stress (Pa) in the axial direction showing the concentration of loading in the core of the pillar

further explanation). These values of rock mass compressive strength were used in the following empirical pillar strength formula (Brady and Brown, 1993):

$$\text{Average Pillar Strength } (\sigma_p) = K_m W^{0.5} H^{-0.7}, \tag{1}$$

where K_m is a unit mass strength (MPa), W is pillar width (m) and H is pillar height (m).

The value of σ_p was adjusted for the effective width (W_e) of a rib pillar (Brady and Brown, 1993):

$$W_e = 4A/P, \tag{2}$$

where A is the plan area of the pillar and P is the pillar circumference.

Using σ_{cm} directly from RocLab as a value for K_m and putting $W = W_e = 2W$ for rib pillars gave the first column of results for σ_p in Table 4. Using the rock mass uniaxial value of σ_c from RocLab as a σ_p value for a square pillar with $W = 2.8$ m and $H = 7$ m in Eq. (1) gave K_m of 21.3 MPa. Again adjusting for $W = 2W$ in Eq. (2) for rib pillars, gave the second column of results for σ_p in Table 4. The average results from the ELFEN modelling are in the third column of σ_p values in Table 4.

In Fig. 21 the results of several simulations described above and empirical results for a variety of pillar types are compared. All are presented as average capacity (stress)

Table 4. Comparison of empirical with modelled average pillar strengths

Width, W (m)	Effective width W_e (m)	Height, H (m)	W/H ratio	σ_p (MPa) $K_m = 13.5$	σ_p (MPa) $K_m = 21.3$	σ_p (MPa) ELFEN
2.8	5.6	7	0.4	8.2	12.9	3 to 8
7	14	7	1.0	12.9	20.4	7 to 15
14	28	7	2.0	18.3	28.9	22 to 27

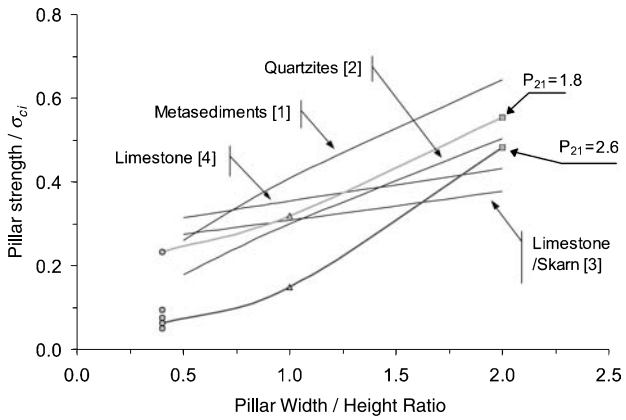

Fig. 21. Comparison between the results of several simulations described in the text and empirical results for a variety of pillar types. All are presented as average capacity (stress) normalised to the intact σ_{ci} values against the pillar width to height ratio. The simulations include a range of P_{21}values from 1.8 to 2.6 m/m^2 and the empirical data show trends for comparable rock materials including metasediments and limestones. Note: (*1*) Von Kimmelmann et al. (1984); (*2*) Hedley and Grant (1972); (*3*) Sjoeberg (1992) and (*4*) Krauland and Soder (1987)

normalised to the intact σ_{ci} values against the pillar width to height ratio. The simulations include a range of P_{21} values from 1.8 to 2.6 m/m^2 and the empirical data show trends for comparable rock materials including metasediments and limestones. Although there are some uncertainties in material parameter values, the magnitudes of the pillar strengths and scale effects are similar.

4. Discussion and Conclusions

4.1 Limitations of Mapping and FracMan Modelling

The mapping area in Middleton was limited to the size of the pillars, with a maximum height of about 8 m. However, only the bottom 2 m was physically accessible for detailed mapping. Above this, the extent of fracture traces must be inferred from photographs. No orientation data is available above the 2 m window. Often, due to poor lighting and air quality, and parallax issues occurring during the photomontage, the condition of the photographs was such that only the most prominent fractures can be conclusively identified. These were usually the longer fractures; shorter fractures (less than about 4 m tracelength) could not be determined in the top half of the face. This must be taken into account when considering the size of window from which to analyse the fracture data, and long and short fractures must be considered on separate scales.

Tests carried out using synthetic data sets in FracMan suggest that for the Middleton rock mass, the P_{21} obtained on a sample plane corresponding to a pillar face can range from 0.8 to 2.3 m/m^2 for a true P_{21} of 1.5 m/m^2. This variability in P_{21} values measured on a small scale has resulted in somewhat inconsistent results from the analyses of the Middleton data. It is sometimes necessary to use a best-estimate intensity to produce a coherent rock mass model. The effect of variations in parameters such as fracture intensity can be explored within the geomechanical modelling.

The sparsity of natural fracture data means that it is often difficult to fit a particular statistical distribution. This is particularly problematic when analysing tracelength data, as shown in Fig. 5. Analytical methods, such as those described by Zhang and Einstein (2000) based on fracture terminations, can be used to determine the appropriateness of particular statistical distributions. However, only 13% of the fractures mapped at Middleton Mine have both ends within the 2 m detailed panel, and 44% have both ends outside the panel. The majority of fractures in set 1a, for example, have both ends outside the visible face, making an estimate of their true trace length uncertain. However, the impact of this on the geomechanical model of pillar behaviour appears to be limited judging by the pattern of extension of the natural fractures.

4.2 Observations from the ELFEN Modelling

The overall progression of failure from the outside of the pillar towards the central core, and the associated stress distributions shown in Figs. 12 to 20 appear to be realistic. There is no direct evidence from an actual field scale pillar failure at Middleton. The debris which results from any pillar failure is mostly inaccessible and

it would be likely impossible to distinguish between small blocks resulting from overstressing in the pillar and small blocks arising from larger ejected blocks that have been subsequently crushed. Further detailed work is needed to examine complete block creation and block sizes during the failure process, and would be most realistic when undertaken in 3D.

It is clear from Fig. 21 that the modelled behaviour indicates a rapidly increasing average strength with increase in W/H ratio. This type of behaviour is more commonly predicted for squat or barrier type pillars at higher W/H ratios (Madden, 1991), but was also seen at similar lower W/H ratios with Hoek-Brown brittle fracture modelling (Martin and Maybee, 2000). While the trend is considered realistic, further parametric studies are required.

Comparison of Figs. 12, 18 and 20 suggests that the influence of the natural fractures diminishes with increasing pillar width, consistent with the strength gain seen in Fig. 21. This is also consistent with observations by Diederichs et al. (2002), who show that in a specific mine the macroscopic pillar behaviour can be modelled with limited consideration of rock structure. This is unlikely to be true in more tensile regimes (hangingwalls, block caving).

It is also clear from Fig. 21 that for slender pillars in particular the value of P_{21} (fracture intensity) has a critical influence on pillar strength. This influence diminishes with increasing pillar width.

The average axial stresses in the Middleton Mine pillars are estimated to be less than 15 MPa. This indicates that the pillar factors of safety could be as high as 2 from the ELFEN model and in the range 1.2 to 2 for a W/H ratio of 2 in Table 4. Factors of safety values are at least 1.5 based on actual condition (Fig. 3) and observations elsewhere on actual pillar behaviour (Diederichs et al., 2002; Lunder and Pakalnis, 1997; Roberts et al., 1998).

The ELFEN model has given overall deformation modulus values for the pillars which are significantly lower than would be predicted by empirical methods – typically in the range 1 to 5 GPa compared with 5 to 15 GPa, per RocLab, using the input data from Tables 1 and 3. This appears to indicate the need to use higher stiffness values and requires further investigation. However, the strain in the pillars, as shown in Fig. 13, is measured from the closure of the whole pillar. At late stages of loading the cross section is much reduced and the inferred local deformation modulus would be higher. It may also be that the unconfined state of the modelled pillars means that there is more freedom for deformation than is implied by the RocLab type of model applied to rock mass rating.

While the results are encouraging in comparison with previous empirical mass strength and width to height ratio models (Table 4 and Fig. 21), the pillar modelling has only been two-dimensional to date. There are two effects, which probably partially compensate, for which three-dimensional modelling will also provide useful insight. In the first place the fractures in the 2D model cross-section are more continuous out of plane than will be the case in 3D. However, in the particular Middleton Mine case example there is substantial real continuity in the major fractures in plane and out of plane, as evidenced by the mapping. The exaggerated out of plane continuity will tend to have led to an underestimate of the pillar strength. Secondly, in a 3D pillar model there is greater freedom for failure to occur due to lack of confinement out of the 2D

plane and this means that the 2D model will tend to have led to an overestimate of the pillar strength.

Another application of 3D characterisation of the rock mass is to improve understanding of the influence of the fracture network on block caving operations. Block caving passes through some well defined stages of block creation and block size reduction. It is possible that future modelling of the type described may be validated against actual block size data (e.g., inferred size and frequency of blocks) from field mapping and FracMan modelling of the undisturbed rock mass, pre-caving and block sizes in drawpoint hang-ups, post-caving.

Based on the modelling results presented to date we believe it is also a realistic objective to examine the geometrical aspects of fracturing (spacing, continuity, orientation) in more detail to provide more control for the rock mass classification approach to mass strength (e.g., RocLab) and excavation stability.

Acknowledgements

The reported work was undertaken as part of a project funded by Engineering and Physical Sciences Research Council (GR/S04970/01) of the United Kingdom. Professor Roger Owen and his team at University of Wales at Swansea were responsible for code developments in ELFEN. Support and material relating to ELFEN and FracMan, were provided by Rockfield Software and Golder Associates respectively. OMYA provided access and logistical support at Middleton Mine. An operating division of Skanska UK Civil Engineering, 3dT, provided the tomographic technology and support for the results in Fig. 10.

References

Bearman, R. A. (1991): The application of rock-mechanics parameters to the prediction of crusher performance. Ph.D. thesis, Camborne School of Mines, Penryn, U.K.

Brady, B. H. G., Brown, E. T. (1993): Rock mechanics for mining, 2nd edn., Chapman and Hall, London.

Cai, M., Kaiser, P. K. (2004): Numerical simulation of the Brazilian test and the tensile strength of anisotropic rocks and rocks with pre-existing cracks. In: Proc., SINOROCK 2004, International Symposium on Rock Mechanics: Rock characterization and, modelling and engineering design methods, 18–21 May, Three Gorges Project site, China. Int. J. Rock Mech. Min. Sci. 41, 450–451.

Coggan, J. S., Pine, R. J., Stead, D., Rance, J. (2003): Numerical modelling of brittle rock failure using a combined finite-discrete element approach: Implications for rock engineering design. In: ISRM 2003 – Technology Roadmap for rock mechanics, South African Institute of Mining and Metallurgy, SAIMM Symposium Series S33. 211–218.

Dershowitz, W. (1992): The role of the Stripa Phase 3 Project in the development of practical discrete fracture modeling technology. In: Proc., Fourth International NEA/SKB Symposium, Stockholm. OECD/NEA, Paris, pp 237–258.

Dershowitz, W., Lee, G., Geier, J., LaPointe, P. R. (1998): FracMan: Interactive discrete feature data analysis, geometric modelling and exploration simulation. User Documentation. Golder Associates Inc., Seattle, Washington.

Dershowitz, W., La Pointe, P., Parney, B., Cladouhos, T. (2001): Multiphase discrete fracture modeling in support of improved oil recovery from the North Oregon Basin, Wyoming.

In: Proc., 38th US Rock Mechanics Symposium, DC Rocks 2001, Washington DC. AA Balkema, Lisse, pp 663–668.

Diederichs, M. S., Coulson, A., Falmagne, V., Rizkalla, M., Simser, B. (2002): Applications of rock damage limits to pillar analysis at Brunswick Mine. In: Hammah, R., Bawden, W., Curran, J., Telesnicki, M. (eds.) Mining and Tunnelling Innovation and Opportunity. Proc. 5th North Am. Rock Mech. Symp. & 17th Tunn. Assn Can. Conf., Toronto, Univ. Toronto Press Toronto.

Eberhardt, E., Stead, D., Coggan, J. S. (2004): Numerical analysis of initiation and progressive failure in natural rock slopes – the 1991 Randa rockslide. Int. J. Rock Mech. Min. Sci. 41, 69–87.

Hedley, D. G. F., Grant, F. (1972): Stope-and-pillar design for the Elliot Lake Uranium Mines. Bull. Can. Inst. Min. Metall. 65, 37–44.

Hoek, E., Carranza-Torres, C., Corkum, B. (2002): The Hoek-Brown failure criterion – 2002. In: 5th North American Rock Mechanics Symposium and 17th Tunnelling Association of Canada Conference, NARMS-TAC 267–271.

Hoek, E., Kaiser, P. K., Bawden, W. F. (1995): Support of underground excavations in hard rock. A.A. Balkema, Rotterdam, 215 pp.

Klerck, P. A. (2000): The finite element modelling of discrete fracture in quasi-brittle materials. Ph.D. thesis, University of Wales, Swansea.

Klerk, P. A., Sellers, E. J., Owen, D. R. J. (2004): Discrete fracture in quasi-brittle materials under compressive and tensile stress states. Comp. Meth. Appl. Mech. Eng. 193, 3035–3056.

Krauland, N., Soder, P. E. (1987): Determining pillar strength from pillar failure observations. Eng. Min. J. 8, 34–40.

Lunder, P. J., Pakalnis, R. C. (1997): Determination of the strength of hard rock mine pillars. CIM Bull, 90 (1013): 51–55.

Madden, B. J. (1991): A re-assessment of coal-pillar design. J. S. Afr. Inst. Min. Metallurgy 90(1), 27–37.

Martin, C. D., Maybee, W. G. (2000): The strength of hard-rock pillars. Int. J. Rock Mech. Min. Sci. 37, 1239–1246.

Owen, D. R. J., Feng, Y. T., Han, K. J. (2000): Finite-discrete element analysis of multi-fracture and multi-contact phenomena. VECPAR 2000, Porto, Portugal, June 21–23, 2000.

Owen, D. R. J., Feng, Y. T., de Souza Neto, E. A., Cottrell, M. G., Wang, F., Andrade Pires, F. M., Yu, J. (2004): The modelling of multi-fracturing solids and particulate media. Int. J. Num. Meth. Eng. 60(1), 317–339.

Owen, D. R. J., Feng, Y. T., Klerck, P. A., Yu, J., Crook, A. J. L. (2001): Computational strategies for multi-fracturing solids and particular media. European Conference on Computational Mechanics, ECCM-2001, Cracow, Poland, June 2001.

Pine, R. J., Berger, E., Hammett, R. D., Artigiani, E. (2004): Vipiteno Mine, Italy – underground mining for marble. Min. Tech. (Trans. Inst. Min. Metall. A). 13, A142–A152.

Roberts, D. P., Lane, W. L., Yanske, T. R. (1998): Pillar extraction at the Doe run Company, 1991–1998. AusIMM 1998 – The Mining Cycle, pp 227–233.

Sjoeberg, J. (1992): Failure modes and pillar behaviour in the Zinkgruvan mine. In: Tillerson, J. A., Wawersik, W. R. (eds.) Proc., 33rd U.S. Rock Mechanics Symp. Santa Fe. Balkema, Rotterdam, 491–500.

Starfield, J. L., Cundall, P. A. (1998): Towards a methodology for rock mechanics modelling. Int. J. Rock Mech. Min. Sci. Geomech. Abstr. 25, 99–106.

Stead, D., Coggan, J. S., Eberhardt, E. (2004): Realistic simulation of rock slope failure mechanisms: the need to incorporate principles of fracture mechanics. In: Proc., SINOROCK 2004, International Symposium on Rock Mechanics: Rock characterization and, modelling and engineering design methods, 18–21 May, Three Gorges Project site, China. Int. J. Rock Mech. Min. Sci. 41, 446.

Von Kimmelmann, M. R., Hyde, B., Madgwick, R. J. (1984): The use of computer applications at BCL Limited in planning pillar extraction and design of mining layouts. In: Brown, E. T., Hudson, J. A. (eds.), Proc., ISRM Symp. Design and Performance of Underground Excavations. Geotechnical Society, London, 53–63.

www.fracman.golder.com. FracMan Technology Group, Golder Associates (UK).

www.rockfield.co.uk/ELFEN.htm. Rockfield Software Ltd. Technium, Kings Road, Prince of Wales Dock, Swansea, SA1 8PH, UK.

Zhang, L., Einstein, H. H. (2000): Estimating the intensity of rock discontinuities. Int. J. Rock Mech. Min. Sci. 37, 819–837.

Zhang, L., Einstein, H. H., Dershowitz, W. S. (2002): Stereological relationship between trace length and size distribution of elliptical discontinuities. Geotechnique 52(6), 419–433.

Authors' address: Professor R. J. Pine, Camborne School of Mines, University of Exeter, Penryn, Cornwall TR10 9EZ, U.K.; e-mail: r.j.pine@exeter.ac.uk